

# Laser-induced water condensation in air

Philipp Rohwetter<sup>1</sup>, Jérôme Kasparian<sup>2\*</sup>, Kamil Stelmaszczyk<sup>1</sup>, Zuoqiang Hao<sup>3</sup>, Stefano Henin<sup>2</sup>, Noëlle Lascoux<sup>3</sup>, Walter M. Nakaema<sup>1</sup>, Yannick Petit<sup>2</sup>, Manuel Queißer<sup>1</sup>, Rami Salamé<sup>3</sup>, Estelle Salmon<sup>3</sup>, Ludger Wöste<sup>1</sup> and Jean-Pierre Wolf<sup>2</sup>

**Triggering rain on demand is an old dream of mankind, with a huge potential socio-economical benefit. To date, efforts have mainly focused on cloud-seeding using silver salt particles. We demonstrate that self-guided ionized filaments generated by ultrashort laser pulses are also able to induce water-cloud condensation in the free, sub-saturated atmosphere. Potential contributing mechanisms include photo-oxidative chemistry and electrostatic effects. As well as revealing the potential for influencing or triggering water precipitation, laser-induced water condensation provides a new tool for the remote sensing of nucleation processes in clouds.**

Global warming and stratospheric ozone depletion have demonstrated that human activities can significantly alter the climate of Earth. However, the potential to locally alter or even control the weather is still the subject of intensive debate<sup>1,2</sup>. There have been long-standing efforts dedicated to seeding clouds<sup>3</sup> with silver salt particles to encourage precipitation. Here, we demonstrate that self-guided ionized filaments<sup>4–8</sup> generated by ultrashort laser pulses are also able to induce water cloud condensation in the free, sub-saturated atmosphere. In additional laboratory experiments under both saturated and sub-saturated conditions, we estimate a water uptake rate of up to  $5 \text{ mg cm}^{-3} \text{ s}^{-1}$  in the active volume of the filament-induced plasma channels. We briefly discuss possible mechanisms that could contribute to this observed laser-induced water condensation, although further investigations are needed to fully clarify their roles. Laser-based condensation provides a new tool for the remote sensing of nucleation processes in clouds and may even open up the possibility of influencing or triggering water precipitation.

Self-guided laser filaments result from a nonlinear propagation regime of ultra-short laser pulses. Beyond a critical power ( $P_{\text{cr}} = 3 \text{ GW}$  in air at a wavelength of 800 nm), the beam self-focuses due to the optical Kerr effect until its intensity is sufficient to allow multiphoton ionization of air molecules, generating a cold plasma. At this point, the released free electrons (typically  $10^{15}–10^{16} \text{ cm}^{-3}$ ) and the negative higher-order Kerr terms<sup>9</sup> tend to defocus the beam and dynamically balance Kerr self-focusing. As a result, one or several self-guided filaments<sup>10</sup> with a diameter of 100  $\mu\text{m}$  are generated over distances much longer than the Rayleigh length, up to hundreds of metres<sup>11</sup>. Filaments can be initiated at predefined remote distances<sup>12</sup> and propagate through adverse conditions including fog and clouds<sup>10</sup>, turbulence<sup>13,14</sup> or reduced pressures<sup>15</sup>. They are therefore well suited for atmospheric applications<sup>4,7</sup>, even in perturbed atmospheres.

We recently demonstrated that laser filaments can trigger corona discharges within thunderclouds<sup>16</sup>, opening the way to lightning control applications. With the present demonstration of water condensation, self-guided filaments also raise new hopes that laser-assisted local weather modification may be achieved, which, in contrast to cloud-seeding using rockets, could be operated continuously and would be free of environmental side effects.

## Experiments

As detailed in the Methods, experiments were conducted both in the free atmosphere and under controlled conditions in a diffusion cloud chamber filled with ambient air. A bundle of 20 to 30 self-guided filaments was generated by the Teramobile femtosecond-terawatt laser<sup>17</sup>, which provided 220-mJ pulses with a duration of 60 fs (3.5 TW peak power) at a central wavelength of 800 nm and a repetition rate of 10 Hz. The filamentation onset was adjusted by providing a negative chirp to the emitted laser pulse, so that the group velocity dispersion (GVD) in the air recompressed the pulse at a distance chosen for the interaction with the air mass under investigation, either in the atmospheric cloud chamber or in the free atmosphere.

## Results and discussion

Highly reproducible filament-induced water condensation trails were observed with the naked eye (see Fig. 1a,b and Supplementary Movie) when the filaments were launched into the atmospheric cloud chamber at a saturation of  $S = 2.3 \pm 0.7$  (that is, a relative humidity,  $\text{RH} = 230 \pm 70\%$ ) and a temperature  $T = -24 \text{ }^\circ\text{C}$ . In ten experiments, we were able to confirm this qualitative observation by recording the corresponding evolution of droplet density and size distribution using a Malvern Spraytec aerosol particle sizer (see typical result in Fig. 1c,d). The particle sizer gave access to particles greater than 2.4  $\mu\text{m}$  only, so the condensation nuclei (CN) and cloud condensation nuclei (CCN) could not be detected. The initial size distribution featured three modes at diameters of 4, 50 and 250  $\mu\text{m}$ . The droplet density in each size class fluctuated significantly due to the residual air turbulence in the chamber and the corresponding inhomogeneous distribution of the pre-existing aerosols. However, a Student  $t$ -test comparing the measured signals before and after the laser shot confirmed that the observed effect has a statistical significance of  $1 - \alpha > 0.9995$ . After the laser was fired, the average diameter of the small particles grew to 6  $\mu\text{m}$ , and their density dropped by half, a change well beyond the fluctuations recorded before the laser pulse. The total water content of this smaller mode therefore remained almost constant. The decrease of this mode is most probably due to the coalescence of droplets, particularly the bigger ones. This coalescence process is sustained by the mutual attraction of

<sup>1</sup>Teramobile, Institut für Experimentalphysik, Freie Universität Berlin, Arnimallee 14, D-14195 Berlin, Germany, <sup>2</sup>Teramobile, GAP, Université de Genève, 20 rue de l'École de Médecine, CH-1211 Genève 4, Switzerland, <sup>3</sup>Teramobile, Université Lyon 1; CNRS; LASIM UMR 5579, bâtiment A. Kastler, 43 Boulevard du 11 novembre 1918, F-69622 Villeurbanne Cedex, France. \*e-mail: jerome.kasparian@unige.ch

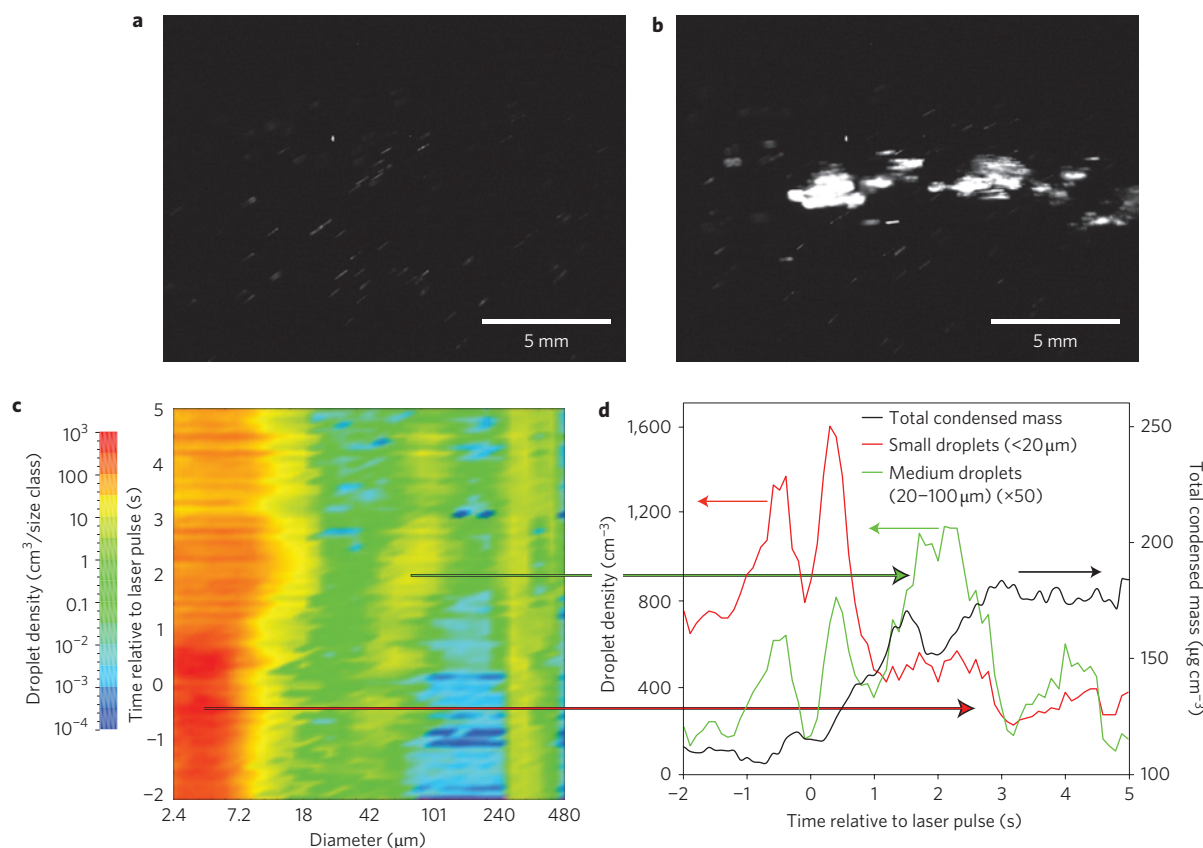


**Figure 1 | Laser-induced condensation in an atmospheric cloud chamber ( $T = -24\text{ }^{\circ}\text{C}$  and  $\text{RH} = 230\%$ ).** **a,b**, View inside the chamber before (**a**) and after (**b**) firing a set of three laser shots at 100-ms intervals. The laser filaments induce macroscopically visible droplet condensation, as is evident from the massive increase in light scattering (see also the Supplementary Movie). **c,d**, Effect of a pair of laser shots launched in the chamber at  $t = 0$  and  $t = 0.1$  s. Temporal evolution of the particle size distribution (**c**) and the amount of small and medium droplets (**d**, left axis) as well as the total condensed water mass (**d**, right axis) per unit volume. The arrows indicate the correspondence between the modes of the size distribution on panel **c**, and the curves displaying their mode-integrated droplet density on panel **d**.

particles bearing opposite net charges generated in amounts of  $10^{15}$ – $10^{16}$  charges  $\text{cm}^{-3}$  by the filaments<sup>18</sup>.

Simultaneously, the density of the mode around  $50\text{ }\mu\text{m}$  doubled. Figure 1c clearly shows that this mode does not develop from smaller droplets, because these two modes remain distinct throughout the growth sequence. Rather, the sudden rise in the medium mode shortly after the laser fired probably stems from the laser-induced fragmentation of droplets from the larger mode at  $250\text{ }\mu\text{m}$ . The  $50\text{-}\mu\text{m}$  droplets then grew to  $80\text{ }\mu\text{m}$  within 3 s. Simultaneously, the biggest mode also grew towards  $400\text{ }\mu\text{m}$ . As a consequence of this growth, the total atmospheric content of condensed water, as determined by integrating the volume of the droplets over the measured size distribution and averaging over the beam, increased by half ( $+70\text{ }\mu\text{g cm}^{-3}$ ). Considering that the  $100\text{-}\mu\text{m}$  filaments only occupy 0.5% of the laser beam volume, the local increase within the filament active volume amounted to a factor of 100 ( $15\text{ mg cm}^{-3}$ ), that is,  $5\text{ mg cm}^{-3}\text{ s}^{-1}$  over the 3 s of growth time. Such results provide clear evidence of filament-assisted condensation. The final droplet diameter of  $80\text{ }\mu\text{m}$  was twice as big as that predicted by a diffusive growth model for pure water under thermodynamically stable conditions<sup>19</sup> (that is, growth limited by the local depletion of water vapour). Their growth rate of  $10\text{ }\mu\text{m s}^{-1}$  was four times faster, probably due to Wilson-type<sup>20</sup> enhancement of the growth rate of the droplets charged by their exposure to the high-charge density generated by the filaments.

However, the Wilson mechanism is not the only mechanism that can explain laser-induced water vapour condensation, because a dramatic and highly reproducible effect was also observed

in sub-saturated conditions (Fig. 2). We varied the relative humidity in the chamber between 70 and 90% and the temperature between 20 and  $60\text{ }^{\circ}\text{C}$ . The observation of an increase in probe light scattering was governed by the water content of the atmosphere rather than by the relative humidity. Condensation was observed only when this was above  $80\text{ }\mu\text{g cm}^{-3}$  provided the relative humidity exceeded 75%. In such conditions, a 30-s series of 300 multifilamenting laser pulses resulted in an immediate rise in the scattering signal by a factor of 10, followed by a slower increase up to a factor of 25 with a time constant  $\tau \approx 4\text{ s}$  (Fig. 2). Such a steep rise again provides clear evidence of an increase in droplet size and number density in the chamber, consistent with observations with the naked eye. Moreover, saturation of the growth rate is typical of a process limited by vapour depletion and the diffusion rate of vapour into the beam region. In contrast, lower water vapour concentrations did not allow substantial condensation even at  $\text{RH} = 95\%$ . The requirement for condensable water before a visible effect is seen shows that it is water vapour condensation indeed that is observed.

This condensation is not affected by the heat deposited by the laser filaments into the air. A typical filament<sup>5–8</sup> with an intensity of  $50\text{ GW cm}^{-2}$ , diameter of  $100\text{ }\mu\text{m}$  and pulse duration of 100 fs carries 0.4 mJ of energy. Even if this energy was totally absorbed over a 10-m length of air, the specific heat of  $1\text{ kJ kg}^{-1}\text{ K}^{-1}$  and the density of  $1.2\text{ kg m}^{-3}$  would yield a temperature increase limited to 3.3 K. In fact, only a small fraction of the filament energy is absorbed, so heating of the air can be neglected in the analysis of our results, and the ambient temperature can be considered as representative of the conditions within the filaments.

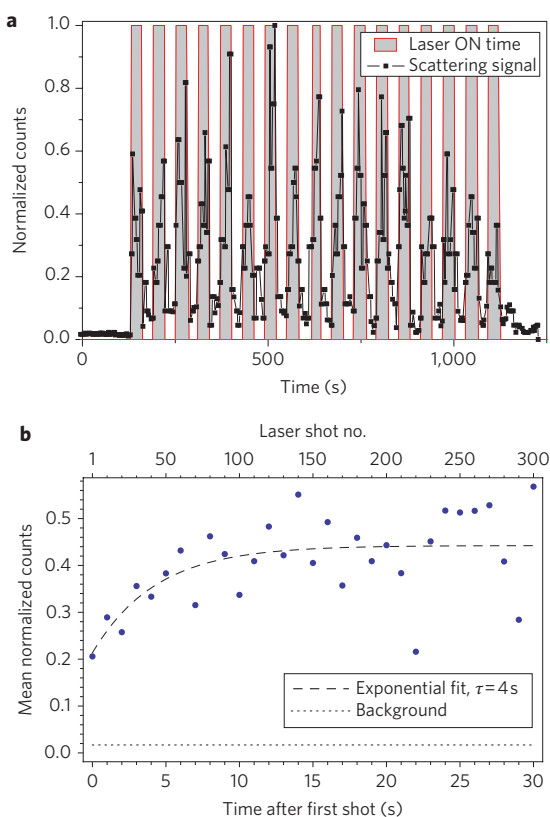


**Figure 2 | Laser-induced condensation in a sub-saturated atmospheric cloud chamber ( $T = 60\text{ }^{\circ}\text{C}$ ,  $\text{RH} = 75\text{--}85\%$ ), observed through the scattered signal at  $90^{\circ}$ .** **a**, High reproducibility of the effect over repeated laser on/off cycles of 300 laser shots each. **b**, Rise time (time constant  $\tau \approx 4\text{ s}$ ) of the light scattered by the growing droplets, averaged over the 17 cycles of panel **a**.

This negligible heating of the air contrasts with the high electron temperature in the plasma filament, which can reach up to 6,000 K (refs 5–8). It should be noted that, due to the small transverse dimension of the filaments, the slight local heating of the air results in large temperature gradients, leading to the development of a shockwave<sup>21</sup>. The corresponding expansion of the air might contribute to the condensation process.

Note also that the fragmentation of pre-existing water droplets into smaller ones increases the scattering signal. We quantified this effect by modelling the laser-induced droplet fragmentation, considering that each mother droplet absorbs an amount of energy proportional to its cross-section, part of which is turned into additional surface energy during fragmentation. A one-step fragmentation model based on a maximum entropy principle results in a Poissonian size distribution of the fragments of each mother droplet<sup>22</sup>. By treating this distribution as continuous, even in cases where it contained only a few tens of daughter particles<sup>23</sup>, we found that the contribution of laser-induced droplet fragmentation to the effect observed in the sub-saturated cloud chamber was marginal, regardless of whether nonlinear absorption or linear absorption were considered. Instead, the observed condensation may be understood by remembering that the atmospheric cloud chamber is filled with ambient air. Therefore, in the urban environment of the laboratory (including aerosols and gaseous pollutants) and in the presence of the high-intensity laser field, photochemically or charge-assisted mechanisms contribute significantly to droplet formation<sup>24–26</sup>.

To provide a definitive demonstration of the capability of laser filaments to trigger condensation, not only in controlled laboratory

conditions but also in real atmospheric conditions, we performed open-field experiments (Fig. 3a) in the late autumn of 2008 in Berlin, Germany, under conditions of polar air mass, providing a high relative humidity ( $\text{RH} = 90\text{--}93\%$ ) together with low level of background aerosols (70 km horizontal visibility). The laser was launched vertically into the atmosphere, at a repetition rate of 5 Hz. The filaments were most active between heights of 45 and 75 m. Their strength then decreased over a few tens of metres beyond this range. The aerosol content of the atmosphere was monitored by LIDAR (light detection and ranging)<sup>27</sup> using a low-power frequency-doubled Nd:YAG laser at 10 Hz repetition rate. This allowed the performance of differential measurements of the changes induced by the terawatt laser pulses preceding the LIDAR pulses (Fig. 3a). The LIDAR return signals provide range-resolved measurements of the total volume backscattering coefficient  $\beta$ , which comprises a molecular contribution (Rayleigh scattering is subtracted in the data processing) and an aerosol contribution (Mie scattering). This aerosol backscattering coefficient  $\beta_{\text{Mie}}$  is defined as<sup>27</sup>

$$\beta_{\text{Mie}} = \int_0^{\infty} N(r) \left. \frac{d\sigma(n, r)}{d\Omega} \right|_{\theta=\pi} dr \quad (1)$$

where  $N(r)$  is the number density of droplets of size  $r$ , and  $d\sigma(n, r)/d\Omega|_{\theta=\pi}$  is the size- and refractive index-dependent backscattering differential cross-section of the particles.  $\beta_{\text{Mie}}$  therefore provides information averaged over all aerosol types and sizes within the probed volume.

The LIDAR measurements were taken 1 ms after firing the terawatt laser pulses. This time delay, much shorter than typical droplet growth times, was imposed by a lateral wind sweeping the air ionized by the filaments out of the detection volume. As already mentioned above, the filaments occupy a fraction of only  $2.5 \times 10^{-4}$  of the air volume probed by the LIDAR. Despite those difficulties and atmospheric fluctuations, the beam-averaged value of  $\beta_{\text{Mie}}$  at the height of the filaments was up to 0.5% higher when following a filamenting laser pulse than without filaments (Fig. 3b). This increase corresponds to a local enhancement of Mie scattering by a factor of 20 within the filaments, from  $\beta_{\text{Mie}} = 1 \times 10^{-6}\text{ m}^{-1}\text{ sr}^{-1}$  to  $2 \times 10^{-5}\text{ m}^{-1}\text{ sr}^{-1}$ . The latter value is typical of haze<sup>27</sup>, in spite of a growth time of 1 ms, much shorter than the signal rise time identified in the sub-saturated chamber (Fig. 2b). Because  $\beta_{\text{Mie}}$  is a measure of all kinds of aerosols, one could argue that only sulphate and nitrate CN or CCN were observed. However, the results of the experiment in the sub-saturated chamber discussed above show that the laser filaments also cause the subsequent condensation of water droplets provided enough water vapour is available in the atmosphere.

The statistical significance of the observed effect was assessed by a Mann–Whitney U-test, comparing the sets of LIDAR signals following a filamenting pulse with the reference LIDAR signals. The null-hypothesis of this non-parametric test is that the two samples are drawn from a single population, so their probability distributions are equal. It therefore makes no assumption about the shape of the underlying distribution(s) and is insensitive to outliers. The Mann–Whitney test can be seen as assessing for differences in medians of the considered distributions. Statistically significant results ( $\alpha < 0.01$ , where  $1 - \alpha$  is the confidence level) were obtained between 6:00 and 6:30, when temperature and relative humidity were  $2.9\text{ }^{\circ}\text{C}$  and 90%, respectively.

Afterwards, the meteorological conditions changed. A reduction in the visibility, a slow increase in the relative humidity up to 93% over 2 h and a rise in the absolute value of the LIDAR signal suggested an increase in the background concentration of water aerosols. Correlatively, the effect of filament-induced condensation on the backscattering signal faded into the background. The fact

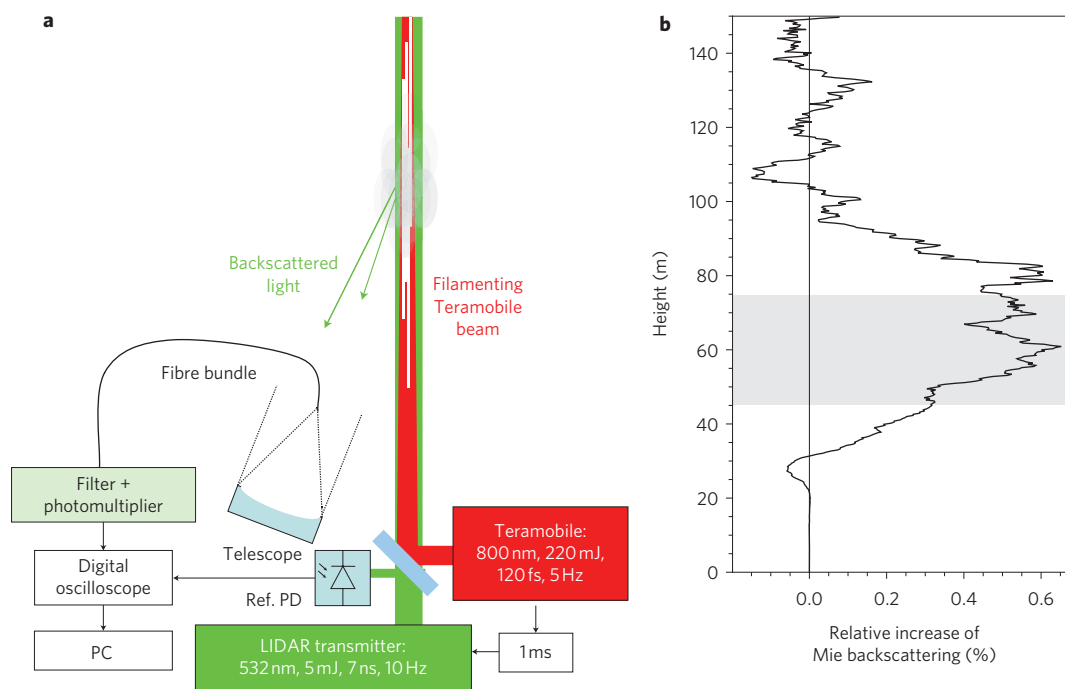


**Figure 3 | Laser-induced condensation experiment in the atmosphere.** **a**, Experimental set-up. The Teramobile laser (red) is fired 1 ms before the LIDAR pulse (green) measuring the aerosol content of the atmosphere. **b**, Time-averaged relative increase of the Mie backscattering coefficient  $\beta_{\text{Mie}}$  measured between 6:00 and 6:30 with and without firing the Teramobile laser. The signal enhancement at the height of the filaments (the most active filamenting region at 45–75 m is shaded) is a clear indication for filament-induced condensation.

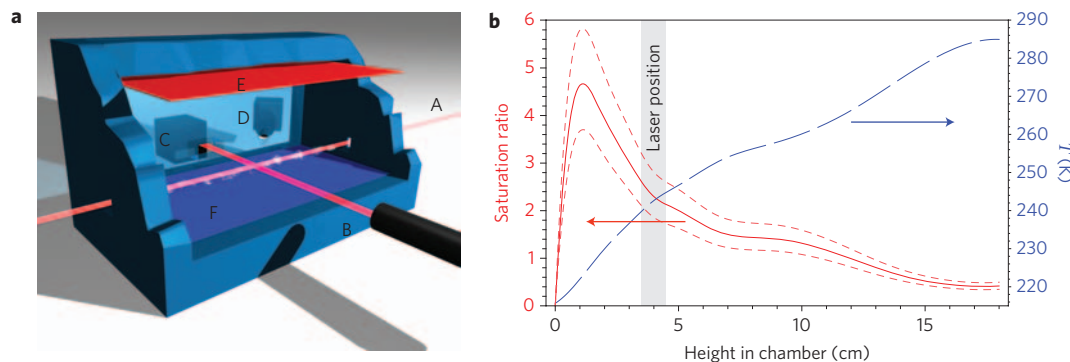


**Figure 4 | Atmospheric diffusion chamber for laboratory experiments.** **a**, Experimental set-up (schematic). A, Teramobile beam; B, particle sizer laser beam; C, particle sizer receiver unit; D, imaging charge-coupled camera; E, heat and vapour source; F, cold bottom plate. **b**, Measured vertical temperature (blue, right scale) and derived supersaturation profile (red, left scale) in the chamber. The dashed lines correspond to the worst-case combinations of  $2\sigma$  temperature and chamber top saturation measurement errors. The grey region indicates the position of the laser beam.

that the observed effects depend on the weather conditions excludes a systematic experimental flaw. Furthermore, we can exclude direct contribution of the filament plasma to the LIDAR signal, because the lifetime of the plasma generated by the filaments does not exceed the microsecond timescale, well below the millisecond interval between the pump and the probe pulses<sup>28</sup>.

As in the cloud chamber experiment, we checked that the enhancement of the LIDAR signal by the laser filaments could not be explained by laser-induced aerosol fragmentation. First, the observed effect decreases when the background LIDAR signal increases, that is, when more water droplets are available for fragmentation. The above-described model of droplet fragmentation quantitatively confirmed this qualitative argument. Based on very high-visibility conditions and air-mass back trajectories<sup>29</sup>, we considered an initial maritime haze size distribution<sup>30</sup>. The visibility provided the water droplet concentration, which was equal to  $136 \text{ mm}^{-3}$ . Alternative rural, remote continental and urban size

distributions were also considered, without affecting the result qualitatively. Between 8 and 400 fragments per mother droplet were considered, with refractive indices in the range 1.3–1.5 commonly encountered in hazes<sup>31</sup>. Even if an overestimation of the filament number (100) and diameter ( $200 \mu\text{m}$ ) were taken into account in the calculations, we found that fragmentation could increase the Mie backscattering coefficient by at most 0.1–0.2%. Thus, fragmentation does not provide the dominant contribution to the observed effect in the atmospheric experiments.

Systematic parametric measurements would be required to better understand and optimize the complex processes at play in our observations. Although such a study is beyond the scope of the present work, some important facts have to be considered. Each filament generates a cold plasma<sup>5–8</sup> with  $10^{15}$ – $10^{16}$  electrons  $\text{cm}^{-3}$  (ref. 5), that is, an average charge generation rate of  $10^{11}$  charges  $\text{cm}^{-3} \text{ s}^{-1}$  at a repetition rate of 10 Hz. Most of these electrons attach to ions within a few picoseconds while, typically,

$10^{13} \text{ cm}^{-3}$  of them attach to  $\text{O}_2$  molecules to form  $\text{O}_2^-$  ions, which last for several microseconds<sup>5</sup>. These oxygen ions can form Wilson clusters<sup>24</sup> with high efficiency due to the extremely high initial concentration of  $\text{O}_2^-$ , even without photoactivation. Direct multiphoton water photolysis<sup>25</sup> can further contribute to this process because the intensity of  $\sim 50 \text{ GW cm}^{-2}$  in the filaments allows processes that are usually only considered for UV lasers. However, thermally driven chemical reactions are not to be considered, because, as discussed above, the plasma generated by the filaments is cold<sup>5–8</sup>.

The exceptionally high charge density could also result in a production rate of oxidizing molecules such as  $\text{O}_3$  and  $\bullet\text{OH}$  radicals that is orders of magnitude above the natural rates found in the atmosphere. The resulting  $\bullet\text{OH}$ , together with the  $\text{O}_2^-$  ions mentioned above, will rapidly produce Wilson clusters<sup>25</sup>, oxidize  $\text{SO}_2$  (refs 26,32) and  $\text{NO}_2$  into  $\text{H}_2\text{SO}_4$  and  $\text{HNO}_3$ , respectively, and assist their heterogeneous nucleation as well as that of volatile organic species. Such processes are indeed compatible with the millisecond timescale of the observed process. Most of these aerosols are highly hygroscopic and will later serve as CCN, allowing the growth of water droplets in adequate humidity conditions, as demonstrated in the sub-saturated cloud chamber experiment. However, at the time of the probe pulse, the scattering efficiencies are still low because the droplets have not had time to grow.

## Conclusions

As a conclusion, we have experimentally demonstrated that self-guided filaments generated by ultrashort laser pulses can assist water condensation, even in an undersaturated free atmosphere. Potential contributing mechanisms include photo-oxidative chemistry and electrostatic effects. The phenomenon provides a new and attractive tool for remote characterization of the humid atmosphere and cloud formation. In addition, it may even provide the potential to influence or trigger water precipitation using continuously operating lasers rather than rockets.

## Methods

The Teramobile femtosecond–terawatt laser<sup>17</sup> used to generate the filaments provided 220-mJ pulses of 60-fs duration at 800 nm, with a repetition rate of 10 Hz. The beam formed a bundle of 20–30 filaments. In laboratory experiments, it was launched through a diffusion chamber<sup>33</sup> (Fig. 4a) filled with ambient air, as single shots or in bursts of up to 30 s in duration. The filaments typically started a few metres before the chamber, which was positioned  $\sim 15$  m away from the laser output. A strong temperature gradient was maintained in the chamber volume of  $0.6 \times 0.3 \times 0.2 \text{ m}^3$  by using a cold base plate that was kept at  $-60^\circ\text{C}$  by indirect contact with a liquid-nitrogen reservoir, and a thermostated circulator heated to  $10^\circ\text{C}$  at the top of the chamber. Water vapour from a reservoir at the top of the chamber diffused towards the bottom plate. We estimated the relative humidity at the top of the chamber to be  $42 \pm 10\%$  by measuring the evaporation time of  $51 \pm 1$  min of sessile water drops with an initial volume of  $2 \mu\text{l}$  (ref. 34). The typical vertical temperature profile, measured with a K-type thermocouple, is shown in Fig. 1b. This profile was used to estimate the supersaturation profile, assuming steady state<sup>35</sup> and a zero water vapour concentration at the bottom of the chamber. The supersaturation was estimated to be  $S \approx 4$  near the bottom of the chamber, consistent with the fact that we operated the chamber slightly below the threshold of sensitivity to cosmic rays<sup>36</sup>. The resulting supersaturation in the interaction region was  $S = 2.3 \pm 0.7$  at a temperature of  $T \approx -24^\circ\text{C}$ . Sub-saturated conditions were obtained by installing a water reservoir that was maintained above  $100^\circ\text{C}$  at the top of the cloud chamber while its bottom was circulator cooled to  $+11^\circ\text{C}$ . The relative humidity at the position of the beam was monitored with a capacitance hygrometer. It ranged between 75 and 85% ( $S = 0.75\text{--}0.85$ ) at a local temperature of  $\sim 60^\circ\text{C}$ .

The water aerosol density in the atmospheric cloud chamber was observed with the naked eye and monitored by launching a low-power continuous wave (c.w.) laser (Nd:YAG, 532 nm, 10 mW) across the path of the pump beam and observing the scattering at  $90^\circ$  or  $45^\circ$ . Scattering is a signature of water droplets, because Rayleigh scattering by air molecules within the cell is negligible at atmospheric pressure over the considered metre scale. Alternatively, the particle size distribution was monitored by measuring the angular distribution of the scattered light of a He:Ne laser in the forward direction using a Malvern Spraytec particle sizer. The data were inverted using Mie theory, while considering the dominant particles to be spherical water droplets.

The atmospheric experiment was performed at night in late autumn of 2008 in Berlin ( $52^\circ 27' 24'' \text{ N}$ ,  $13^\circ 17' 38'' \text{ E}$ , 55 m above sea level), under conditions of

incoming arctic cold air ( $2.9^\circ\text{C}$ ) and initially strong westerly winds at an atmospheric pressure of  $\sim 995$  hPa, with a relative humidity initially stable at 90% over 1 h and then slowly rising to 93% over 2 h. The horizontal visibility and wind speed and direction were measured 33 and 39 m above ground, respectively, 1,140 m east of the experimental location. Temperature and relative humidity were recorded upwind at 620 m in the east–south–east direction away from the experimental site. The initial horizontal standard visibility was  $\sim 70$  km, indicating an exceptionally low background of aerosol scatterers. This value was used to calibrate the aerosol-related fraction of the atmospheric backscattering coefficient from the LIDAR signals.

In this experiment (Fig. 3), the Teramobile beam was expanded to a diameter of 10 cm and launched vertically into the free atmosphere at a repetition rate of 5 Hz. The pulses were chirped and the beam slightly focused to maximize the strength of multiple filamentation at a distance of 60 m. Backscattering from the atmosphere was probed with a LIDAR using a 5-mJ YAG laser beam at 532 nm, pulsed at 10 Hz, emitted collimated with a beam diameter of 4 cm, and overlapped with the Teramobile beam on a dichroic mirror. This overlap was checked at 0 and 60 m by folding the beams horizontally, ensuring that the strongly filamenting region was effectively superposed with the probe beam.

The probe beam alternately measured the backscattering 1 ms following a Teramobile shot and then in unaffected atmosphere 100 ms following the shot. The horizontal wind speed of  $2.5\text{--}5 \text{ m s}^{-1}$  ensured that each pulse (resp. pulse pair) interacted with a fresh air column. Single-shot LIDAR transients were collected with a 11.4-cm-diameter,  $f = 500$  mm telescope (4 mrad field of view), 20 cm off the axis of the laser beam, detected by a photomultiplier tube equipped with a narrowband (1 nm bandwidth full-width at half-maximum (FWHM) at 532 nm) interference filter, and recorded on a digital oscilloscope used as a transient recorder (500 MHz bandwidth). Each individual LIDAR signal was normalized by the pulse energy of the probe pulses, as recorded using a high-speed photodiode. The inclination between the axes of the laser beams and of the telescope provided 100% overlap around 60 m, in the filamenting region. We integrated the LIDAR signals generated by probe pulses over the most active filamenting region, between altitudes of 45 and 75 m (shaded region of Fig. 3), and compared those following a Teramobile pulse with reference pulses.

Received 11 November 2009; accepted 8 March 2010;  
published online 2 May 2010

## References

- Qiu, J. & Cressey, D. Taming the sky. *Nature* **453**, 970–974 (2008).
- US National Research Council. *Critical Issues in Weather Modification Research* (National Academies, 2003).
- Langmuir, I. Growth of particles in smokes and clouds and the production of snow from supercooled clouds. *Science* **106**, 505 (1947).
- Kasparian, J. *et al.* White-light filaments for atmospheric analysis. *Science* **301**, 61–64 (2003).
- Couairon, A. & Mysyrowicz, A. Femtosecond filamentation in transparent media. *Phys. Rep.* **44**, 47–189 (2007).
- Bergé, L., Skupin, S., Nuter, R., Kasparian, J. & Wolf, J.-P. Ultrashort filaments of light in weakly-ionized, optically-transparent media. *Rep. Prog. Phys.* **70**, 1633–1713 (2007).
- Kasparian, J. & Wolf, J.-P. Physics and applications of atmospheric nonlinear optics and filamentation. *Opt. Express* **16**, 466–493 (2008).
- Chin, S. L. *et al.* The propagation of powerful femtosecond laser pulses in optical media: physics, applications and new challenges. *Can. J. Phys.* **83**, 863–905 (2005).
- Béjot, P. *et al.* Higher-order Kerr terms allow ionization-free filamentation in air. *Phys. Rev. Lett.* **104**, 103903 (2010).
- Méjean, G. *et al.* Multifilamentation transmission through fog. *Phys. Rev. E* **72**, 026611 (2005).
- La Fontaine, B. *et al.* Filamentation of ultrashort pulse laser beams resulting from their propagation over long distances in air. *Phys. Plasma* **6**, 1615–1621 (1999).
- Rodriguez, M. *et al.* Kilometer-range non-linear propagation of femtosecond laser pulses. *Phys. Rev. E* **69**, 036607 (2004).
- Chin, S. L. *et al.* Filamentation of femtosecond laser pulses in turbulent air. *Appl. Phys. B* **74**, 67–76 (2002).
- Salamé, R., Lascoux, N., Salmon, E., Kasparian, J. & Wolf, J.-P. Propagation of laser filaments through an extended turbulent region. *Appl. Phys. Lett.* **91**, 171106 (2007).
- Méchain, G. *et al.* Propagation of fs-TW laser filaments in adverse atmospheric conditions. *Appl. Phys. B* **80**, 785–789 (2005).
- Kasparian, J. *et al.* Electric events synchronized with laser filaments in thunderclouds. *Opt. Express* **16**, 5757–5763 (2008).
- Wille, H. *et al.* Teramobile: a mobile femtosecond–terawatt laser and detection system. *Eur. Phys. J.—Appl. Phys.* **20**, 183–190 (2002).
- Kasparian, J., Sauerbrey, R. & Chin, S. L. The critical laser intensity of self-guided light filaments in air. *Appl. Phys. B* **71**, 877–879 (2000).
- Pruppacher, H. R. & Klett, J. D. *Microphysics of Clouds and Precipitation* (Kluwer Academic Publishing, 1997).

20. Wilson, C. T. R. On a method of making visible the paths of ionising particles through a gas. *Proc. R. Soc. Lond. A* **85**, 285–288 (1911).
21. Yu, J. *et al.* Sonographic probing of laser filaments in air. *Appl. Opt.* **42**, 7117–7117 (2003).
22. Cohen, R. D. Shattering of a liquid drop due to impact. *Proc. R. Soc. Lond. A* **435**, 483–503 (1991).
23. Villiermaux, E. Fragmentation. *Annu. Rev. Fluid Mech.* **39**, 419–446 (2007).
24. Byers Brown, W. Photonucleation of water vapour in the presence of oxygen. *Chem. Phys. Lett.* **235**, 94–98 (1995).
25. Clark, I. D. & Noxon, J. F. Particle formation during water-vapor photolysis. *Science* **174**, 941–944 (1971).
26. He, F. & Hopke, P. K. SO<sub>2</sub> oxidation and H<sub>2</sub>O–H<sub>2</sub>SO<sub>4</sub> binary nucleation by radon decay. *Aerosol Sci. Technol.* **23**, 411–421 (1995)
27. Measures, R. M. *Laser Remote Sensing—Fundamentals and Applications* (Wiley Interscience, 1984).
28. Tzortzakakis, S., Prade, B., Franco, M. & Mysyrowicz, A. Time evolution of the plasma channel at the trail of a self-guided IR femtosecond laser pulse in air. *Opt. Commun.* **181**, 123–127 (2000).
29. Aeronet project, NASA, back trajectory data for stations Leipzig (D), Hamburg (D), and Belsk (PL), <http://croc.gsfc.nasa.gov/aeronet/>.
30. Jaenicke, R. Tropospheric aerosol, in *Aerosol–Cloud–Climate* (Hobbs, P. V., ed.) (Academic Press, 1993).
31. Quentzel, H., Ruppertsberg, G. H. & Schellhase, R. Calculations about the systematic error of the visibility-meters measuring scattered light. *Atmos. Environ.* **9**, 587–601 (1975).
32. Caffrey, P. *et al.* In-cloud oxidation of SO<sub>2</sub> by O<sub>3</sub> and H<sub>2</sub>O<sub>2</sub>: cloud chamber measurements and modelling of particle growth. *J. Geophys. Res.* **106**, 27587–27601 (2001).
33. Langsdorf, A. Jr. A continuously sensitive diffusion cloud chamber. *Rev. Sci. Instrum.* **10**, 91–103 (1939).
34. Schönfeld, F., Graf, K. H., Hardt, S. & Butt, H. J. Evaporation dynamics of sessile liquid drops in still air with constant contact radius? *Int. J. Heat Mass Transfer* **51**, 3696–3699 (2008).
35. Saavedra, I. On the theory of the diffusion cloud chamber. *Nucl. Instrum.* **3**, 85–89 (1958).
36. Tohmfor, G. & Volmer, M. Die keimbildung unter dem einfluß elektrischer ladungen. *Annalen der Physik* **425**, 109–131 (1938).

### Acknowledgements

The authors would like to acknowledge J. Kirkby of CERN for fruitful discussions, I. Sorge of Institut für Meteorologie, FU-Berlin, Germany, for providing weather data, and T. L. Kucsera (GEST) at NASA/Goddard for back-trajectories (available at the [aeronet.gsfc.nasa.gov](http://aeronet.gsfc.nasa.gov) website). This work was supported by the Deutsche Forschungsgemeinschaft, Agence Nationale de la Recherche (Project ANR-05-Blan-0187), the Fonds National Suisse de la Recherche Scientifique (FNS, grant nos. 200021-116198 and 200021-125315), and the Swiss Secrétariat d'État à l'Éducation et à la Recherche in the framework of the COST P18 project 'The Physics of Lightning Flash and its Effects'.

### Author contributions

All authors contributed extensively to the work presented in this paper. More specifically, P.R., J.K., K.S., L.W. and J.-P.W. conceived and designed the study. P.R., K.S., Z.H., S.H., N.L., W.N., Y.P., M.Q., R.S. and E.S. performed the experiments. P.R., J.K. and K.S. analysed the data, and J.K., L.W. and J.-P.W. wrote the paper.

### Additional information

The authors declare no competing financial interests. Supplementary information accompanies this paper at [www.nature.com/naturephotonics](http://www.nature.com/naturephotonics). Reprints and permission information is available online at <http://npg.nature.com/reprintsandpermissions/>.

Correspondence and requests for materials should be addressed to J.K.